TUDelft

Delft University of Technology

In-series sample methodology for permeability characterization demonstrated on carbon nanotube-grafted alumina textiles

Staal, Jeroen; Caglar, Baris; Hank, Travis; Wardle, Brian L.; Gorbatikh, Larissa; Lomov, Stepan V.; Michaud, Véronique

Important note
To cite this publication, please use the final published version (if applicable).
Please check the document version above.

In-series sample methodology for permeability characterization demonstrated on carbon nanotube-grafted alumina textiles

Jeroen Staal [a,b], Baris Caglar [a,c], Travis Hank [d], Brian L. Wardle [d,e], Larissa Gorbatikh [b], Stepan V. Lomov [b], Véronique Michaud [a,*]

[a] Laboratory for Processing of Advanced Composites (LPAC), Institute of Materials (IMX), Ecole Polytechnique Fédérale de Lausanne (EPFL), Station 12, Lausanne CH-1015, Switzerland
[b] Department of Materials Engineering, KU Leuven, Kasteelpark Arenberg 44, Heverlee, Belgium
[c] Aerospace Manufacturing Technologies, Faculty of Aerospace Engineering, Delft University of Technology, Kluyverweg 1, Delft 2629HS, the Netherlands
[d] Department of Aeronautics and Astronautics, Massachusetts Institute of Technology, 77 Massachusetts Ave, Cambridge, MA 02139, United States
[e] Department of Mechanical Engineering, Massachusetts Institute of Technology, 77 Massachusetts Ave, Cambridge, MA 02139, United States

ARTICLE INFO

ABSTRACT

In-plane permeability of small area (100 × 50 mm) alumina fiber woven fabrics grafted with aligned carbon nanotubes (CNT) was quantified by placing them in series with a glass mat of known permeability during a flow experiment. The methodology was first validated on a reference woven textile. Permeability values matched those obtained by a direct method within a margin of ±15%. Permeabilities of radial-aligned (short CNT, SCNT) and so-called 'Mohawk' (long CNT, LCNT) morphologies of the CNT-grafted samples were then measured and compared to the non-grafted alumina, showing a decrease attributed to a change in local textile structure as assessed in previous studies. Unsaturated permeability decreased by 77% after SCNT- and 88% after LCNT-grafting, while saturated permeability further decreased by 90% and 93%, respectively. The high ratio of unsaturated to saturated permeability (in the range of 1.14 – 2.89) implies that capillary wicking contributes largely to the impregnation of CNT-grafted fabrics.

1. Introduction

Nano-scale reinforcements can be used to enhance fiber reinforced polymers (FRPs), where carbon nanomaterials, including CNTs [1] and graphene [2], have received the main research attention to date. Addition of carbon nanotubes (CNTs) has repeatedly been reported to result in enhanced mechanical, thermal and electrical performance [3–7] of FRPs. Grafting these CNTs onto the fiber surface [8–11] has been shown to be the most advantageous technique over dispersion in the matrix [12–15] or in the fiber sizing [16,17]. Main benefits of grafting are high CNT weight fractions and a good control of orientation [3], while overcoming difficulties in matrix infiltration due to resin viscosity increases, and CNT agglomeration. Variations in grafting methodologies typically result in different CNT forests morphologies [8]. The procedure reported, amongst others, by Yamamoto et al. [8], Wicks et al. [18] and Aravand et al. [19] allows grafting of so-called 'fuzzy', closely-spaced, uniformly aligned CNT forests onto ceramic fiber surfaces. The CNT forests showed 'Mohawk'-morphologies, where the CNTs form several distinct clusters due to inter-CNT van der Waals forces. CNT lengths in such forests exceeded the fiber diameter [8] while smaller CNT lengths resulted in uniform orientations perpendicular to the fiber surface, i.e. radial morphology. The most prominent mechanical enhancement was in the inter- and intralaminar properties, e.g. Mode I interlaminar fracture toughness increased by up to 76% [18] after radially aligned grafting and 100% [20] after 'Mohawk' grafting.

Scaling up these enhanced properties to an industrial scale demands a detailed understanding of the processing conditions, to predict process cycle times and to obtain reproducibly sound materials [21]. The quality of parts produced by Liquid Composite Molding strongly depends on the infiltration behavior of the matrix material into the textile preform, which is characterized by its permeability tensor **K**. Linear measurements of saturated and unsaturated permeability are commonly exploited for quantitative characterization of this behavior. Saturated permeability is obtained by measuring the flow rate of a model fluid flowing through the preform, while the so-called unsaturated permeability of fabric specimens is measured from the position of the fluid flow

front over time. The latter is often used in practice, and provides results that are close to the saturated permeability if the capillary forces at the flow front are sufficiently low [22]. It is commonly characterized by means of the squared flow front (SFF) methodology [23], provided that the aspect ratio of in-plane dimensions surpasses a threshold of 3:1 [24]. Several methods have been proposed to increase experimental efficiency of unsaturated permeability analysis, so as to reduce the number of specimens to fully characterize a textile in various conditions. Di Fratta et al. [25] proposed a method for characterization of sequentially placed fabric sections with varying fiber volume fractions (V_f) based on distribution of flow front progression observations over the sample length. The approach developed by Dong et al. [26] made use of a control volume finite element (CVFE) method based on imaged flow front progression data. This method made it possible to derive unsaturated permeabilities of sections with both different V_f and fiber architectures, but

significant error accumulation limited the accuracy and possible number of fabrics. Caglar et al. [22] overcame these issues in their CVFE approach, which allowed an accurate derivation of the 2D permeability distribution of individual elements. This approach is the basis for the current work and a detailed explanation of the methodology can be found in Section 2.4.

Only few reports are dedicated to the permeability of the aforementioned 'fuzzy' textiles. Lomov et al. [27] used a linear permeability setup to characterize the unsaturated permeability of low-density CNT grafted textiles. Grafting of CNTs was found not to influence the permeability if the volume of individual CNTs was taken into account in the V_f calculations. Lidston et al. [28] and Wicks et al. [29,30] reported on the processing of high-density CNT grafted textiles in a vacuum assisted resin infusion (VARI) setup. They observed a strong decrease of an order of magnitude [29,30] in the flow front kinetics in the grafted

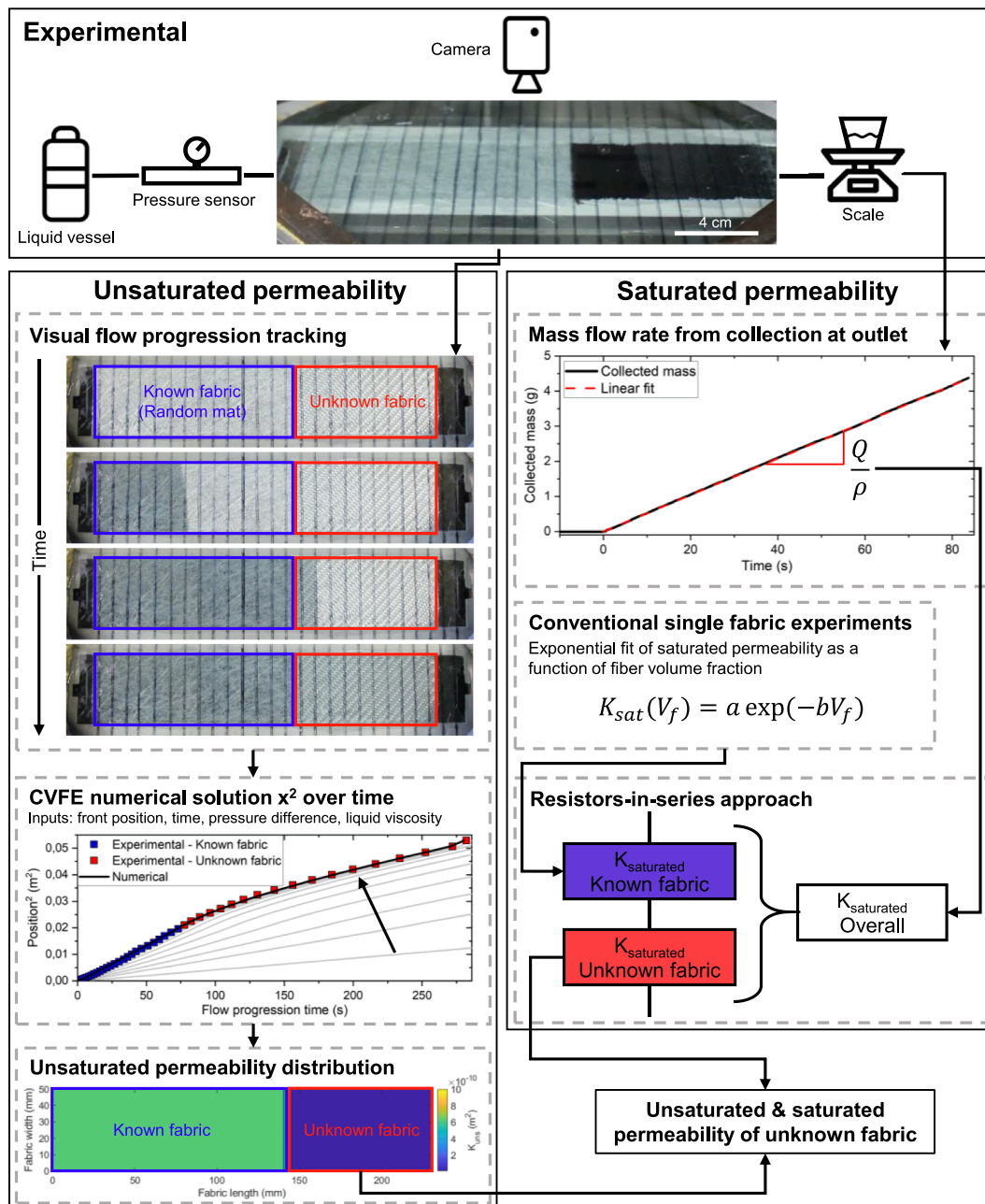
Fig. 1. Schematic representation of developed in-series sampling methodology for permeability characterization. (For interpretation of the references to colour in this figure legend, the reader is referred to the web version of this article.)

fabrics. This decrease was observed to be independent of the added weight fraction by CNTs, which contradicts theoretical permeability relations that predict a decrease of permeability with increasing surface area [28], and thereby increasing CNT charge. No work to date has been reported on the permeability characterization of high-density CNT-grafted textiles. This is in large part due to the lack of a dedicated set-up, as the CNT-grafted fabrics are produced in lab-scale devices in small quantities, which are often not adapted to the large sample size required in permeability measurement set-ups to reach a steady flow (generally, minimum 20 cm long [23]). Overcoming this would pave a way towards an improved understanding of processing behavior to maximize the benefits obtained after CNT grafting.

In this article we propose a methodology that allows unsaturated and saturated permeability characterization of fabric stacks that do not allow production of samples with sizes and aspect ratios (i.e. sample length to sample width) sufficient to fulfil the testing requirements [23]. The basic concept, represented in Fig. 1, is to place the fabric of interest in series downstream of a fabric of known permeability, so as to back-calculate its permeability from the overall result. The feasibility of this methodology is first validated in a system containing two types of glass fabrics whose permeabilities are independently characterized with well-established unidirectional permeability characterization experiments. It is then exploited for the permeability characterization of 'fuzzy' textiles with different CNT configurations.

2. Materials and experimental methods

2.1. Materials

A model system for methodology development consisted of an isotropic random glass mat and a 2x2 twill E-glass fabric (both from Suter Kunststoffe AG) with a glass fiber bulk density of 2.60 g/cm^3 and areal density of the fabrics of 450 g/m^2 and 390 g/m^2, respectively, with microstructures shown in Fig. 2a and 2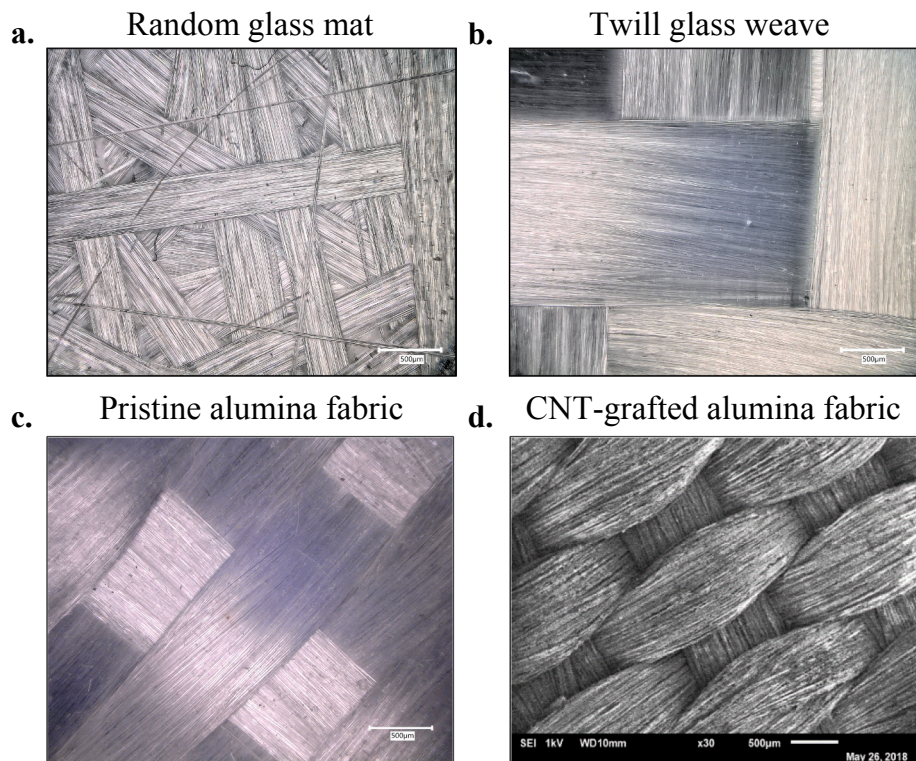b. Linear densities of the yarns in the woven fabrics were 340 tex in warp and 272 tex in weft with ends/picks count of 6/6.7 yarns/cm. CNTs were grafted on a plain woven alumina fabric tape (Cotronics Ultra Temp 391), as used by e.g. Aravand et al. [19] and Lomov et al. [31], with an areal density of 371 g/m^2, a linear density of the yarns 221 tex in both warp and weft direction, and ends/picks count of 11.9/4.9 yarns/cm. Examples of pristine and CNT-grafted alumina fabrics are shown in Fig. 2c and 2d, respectively.

Two model fluids have been used for permeability measurements: an aqueous poly(ethylene glycol) (PEG) solution for the model system and silicon oil (Dow Corning Xiameter PMX 200/100 cS, VWR Chemicals) for alumina-based fabrics. An overview of the main liquid properties and activation energies is given in Table 1. The PEG solution consisted of 16.7% by weight of PEG (M_w = 35 kDa, Sigma Aldrich) and a few drops of food colorant to enhance optical contrast. Corresponding viscosity values are reported in Ref. [32]. Viscosity of the silicone oil was measured in a concentric cylinder rheometer (AR2000ex, TA Instruments) under continuous shear. Temperatures varied between 15 °C and 25 °C and viscosity was fitted with an Arrhenius relation [32], relating the liquid viscosity η with frequency factor A, activation energy E_a, gas constant R and the temperature T:

$$\eta(T) = A\exp\left(-\frac{E_a}{RT}\right) \tag{1}$$

Table 1
Overview of main liquid properties of the used model fluids.

Fluid	Density g/cm^3	Viscosity (η) (20 °C) Pa s	A Pa s	E_a kJ K^{-1} mol^{-1}
PEG	1.026	0.111	$2.312 \cdot 10^{-5}$	20.67
Silicon oil	0.964	0.101	$2.773 \cdot 10^{-4}$	14.37

a. Random glass mat

b. Twill glass weave

c. Pristine alumina fabric

d. CNT-grafted alumina fabric

Fig. 2. Optical and SEM images of the microstructure of the used fabrics: (a) Random glass mat reference fabric, (b) twill glass weave, (c) Pristine alumina fabric, (d) CNT-grafted alumina fabric.

2.2. CNT-growth onto alumina textiles

CNT-growth of aligned CNTs was carried out following the methodology that was previously reported in Refs. [8,18,19,31], while growth times were different. Alumina fabrics were soaked in a 50 mM iron nitrate ($Fe(NO_3)_3 \cdot 9H_2O$, Alfa Aesar) catalyst solution in isopropanol followed by overnight drying at 30 °C. Fabrics were then cut into 100 x 50 mm swatches and placed in the middle of a ~5 cm inner diameter tube furnace (Lindberg Blue M). Reduction to iron nanoparticles was done under hydrogen flow at a furnace setpoint of 650 °C for 8 min. CNTs were grown by chemical vapor deposition at 650 °C by means of an ethylene (C_2H_4) source. Radial CNTs (SCNTs) were grown during a 2.1 min ethylene exposure, while 'Mohawk'-morphologies (LCNTs) were grown with 4.4 min exposure time. The resulting CNT-morphology is shown in Fig. 3.

2.3. Conventional unidirectional permeability

Permeability was characterized in a linear flow test setup, consisting of a rigid mold with a transparent glass top and an injection unit. Fabric stacks were surrounded by a silicon seal and placed within a metallic spacer. Spacer height was adjusted for non-grafted alumina, SCNT and LCNT fabrics to ensure the compression did not reach the stress limit of the mold [31]. Mold halves were compressed at 2 bars after closure by inflation of two air cushions. Model fluids were pressurized with compressed air in a pressure vessel to obtain a constant pressure difference over the fabric. A small pressure gradient of 0.18 bar was chosen to preserve the grafter fabrics microstructure, in turn possibly enhancing the relative magnitude of capillary pressure, which is typically in the kPa range [33–36]. The pressure and temperature were recorded at 250 Hz by a pressure sensor (Keller Series 35XHTT), which was placed between the liquid reservoir and the inlet. Flow front progression was recorded by a camera (Canon EOS700D) at 30 fps. Quantitative analysis was then possible based on the relative times of the flow front passing 1 cm spaced lines perpendicular to the flow direction. Liquid at the outlet was collected and continuously weighed with a Mettler PM2500 scale (±0.1 mg accuracy), connected to a computer. An image of the experimental setup can be found in Supplementary Information S1.

Regular linear flow experiments were conducted for all non-grafted fabric types; isotropic random glass mat, 2x2 twill E-glass fabric, and woven alumina fabric. Stacks of 250 x 50 mm fabric patches of a single fabric type were placed in the mold cavity. The number of layers per stack were varied to derive the permeability-V_f relations. V_f-values were calculated from the fabric weight before each measurement. Unsaturated permeability calculations were carried out following the Squared Flow Front (SFF) approach [23], which relates the permeability (K_{SFF}) with the in-plane flow under constant applied pressure as:

$$K_{SFF} = -\frac{m(1 - V_f)\eta}{2\Delta P} \tag{2}$$

where m is the slope of the squared flow front progression over time, V_f the fiber volume fraction, η the liquid viscosity and ΔP the applied pressure gradient over the fabric, averaged over the experimental running time. Data belonging to the first few centimeters was excluded from the analysis as transient effects such as pressure build-up was still present when test fluid reached the fabric.

Saturated permeability (K_{sat}) was derived from the volumetric flow rate at the liquid outlet, Q, that was calculated from the slope of collected liquid mass over time and the liquid density. Calculation was then done with the following relation:

$$K_{sat} = \frac{Q\eta L}{S\Delta P} \tag{3}$$

where L is the fabric length, η the liquid viscosity, S the cross-sectional area of the fabric stack and ΔP the pressure gradient over the fabric stack. Data points were taken after the flow had stabilized over a period of 60–100 s.

Characterization was carried out over a range of V_f-s for all fabrics, after which both unsaturated and saturated permeability were fitted

Radially aligned CNT-grafting

'Mohawk' CNT-grafting
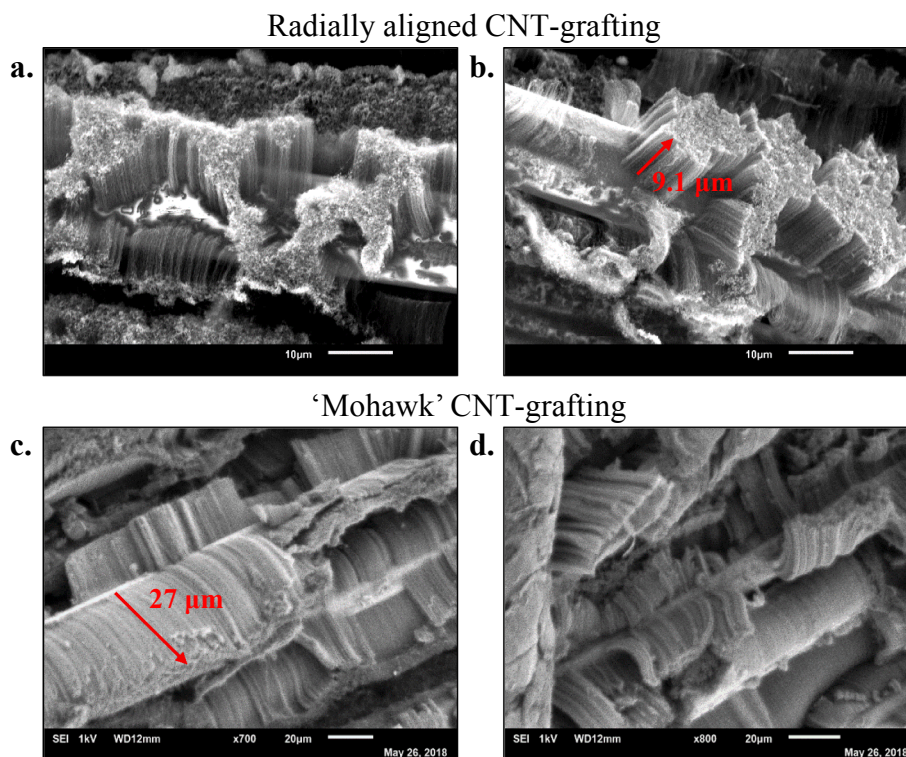
Fig. 3. CNT-morphologies of (a,b) radially aligned CNT-grafted textiles and (c,d) 'Mohawk' CNT-grafted textiles. (For interpretation of the references to colour in this figure legend, the reader is referred to the web version of this article.)

with an exponential relation where a and b are fitting parameters:

$$K_{fit} = a\exp\left(-bV_f\right) \tag{4}$$

2.4. Sequential permeability experiments

The conventional methodologies were then extended to a series-approach to allow the characterization of fabrics that do not fulfil the typical size and aspect ratio requirements. These experiments were built-up using a 100×50 mm stack of the fabric of interest, corresponding to the dimension of the available CNT-grafted alumina fabrics, that was preceded by a 140×50 mm stack of isotropic random glass mat to ensure it fits within the 250 mm mold cavity when transition regions between fabrics are non-optimal.

A simplified strategy for unsaturated permeability characterization was developed based on the methodology previously reported by Caglar et al. [22]. One-dimensional CVFE elements of 5 mm length, as validated and used in Ref. [22] for similar flow scenarios, were created by the interpolation of the flow progression curve in flow direction and control volumes were defined at the element centers. V_f-s were assigned to individual nodes based on the fabric they correspond to. These V_f-s were experimentally chosen to give the first section a higher unsaturated permeability than the second one, as this is required to minimize the prediction error of the CVFE methodology [22,25]. A Levenberg-Marquardt [37,38] optimization algorithm was used to derive an unsaturated permeability value for both fabrics simultaneously. This optimization procedure is schematically illustrated in Fig. 1. Both fabrics were assigned an initial guess on its permeability value, while a small transition region was created between them. Calculation of numerical element fill times comprised the approximation of the pressure distribution, taking into account boundary conditions at the extremes of the mold. Elements were set to be first order to ensure continuity of the

pressure distribution. Control volumes at the flow front were used to calculate the volumetric flux via Darcy's law, from which the fill time of the next element was derived. This continued until the mold was filled and the whole filling procedure was iteratively repeated until the numerical fill times closely matched the experimental transient flow front positions. The reader is referred to the article of Caglar et al. [22] for further details on the numerical procedure.

Regarding the saturated permeability of different fabric types placed in series, a resistors-in-series formula was simply used to evaluate the permeability of the measured fabric:

$$K_{sat,2} = \frac{L_2}{\frac{L_{1+2}}{K_{sat,1+2}} - \frac{L_1}{K_{sat,1}}} \tag{5}$$

where K_{sat} is the saturated permeability, L the fabric length with subscripts 1 and 2 for the first and second fabric stacks in flow direction, respectively. The overall saturated permeability was calculated analogously to the reference experiments, with use of Eq. (3). Previously established exponential permeability-V_f relations were used to predict the saturated permeability of the isotropic random glass mat stack ($K_{sat,1}$), leaving the permeability of the subsequent fabric stack as the only unknown.

3. Results

The developed strategy for unsaturated and saturated permeability characterization was first validated on the model system consisting of the twill weave glass fabric as sample fabric, preceded by the isotropic random mat stack. A comparison of the fabrics-in-series methodology with baseline permeability results obtained with a single fabric is shown in Fig. 4. Exponential permeability-V_f relations were fitted to the results of single fabric unsaturated and saturated permeability measurements,
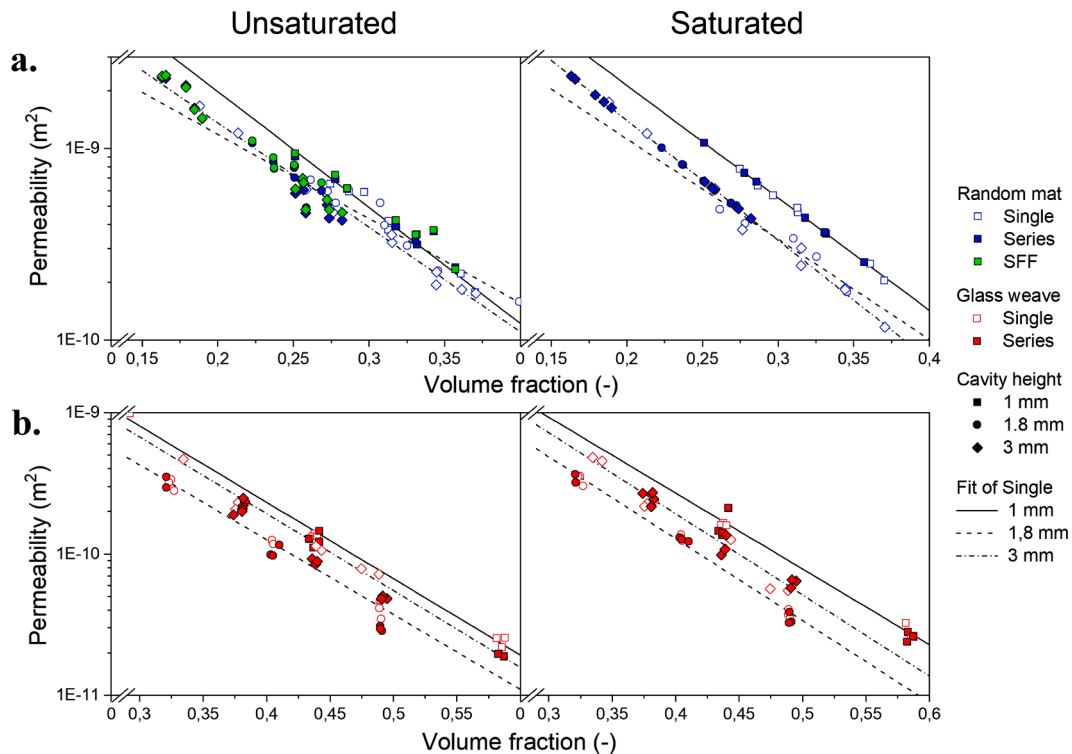
Fig. 4. Overview of series-derived permeability values of the model system, compared to conventional single fabric reference experiments: (a) unsaturated and saturated permeability of the isotropic random mat, (b) unsaturated and saturated permeability of the twill glass weave fabric. Notations single (empty markers) and series (filled markers) refer to experimental values obtained following the conventional approach with single fabric type and the CVFE approach with a random mat fabric and a glass weave fabric in series, respectively. In (a), SFF refers to the Squared Flow Front approach for unsaturated permeability calculation. (For interpretation of the references to colour in this figure legend, the reader is referred to the web version of this article.)

with varying cavity height and fabric type. The range of V_f-s that could be covered for a certain cavity height was limited by the possible number of layers in a fabric stack. The lower bound of this number depends on the uncompressed fabric layer thickness, to ensure sufficient friction with the mold wall to prevent the fabrics moving in flow direction. The upper bound was determined by the maximum allowed stresses for the linear flow mold.

Thickness effects were found to be present as the exponential fits showed differences between the considered mold cavity heights. These observed differences were attributed to fabric-related sources because the curves showed larger differences between fabric types in Fig. 4a and in 4b, while the shape of the fitted exponential curves was relatively similar for unsaturated and saturated cases. In particular for 1 mm stacks, the permeability tends to be overestimated. This is probably due to reduced nesting and more dominant surface boundary effects, leading to a greater uncertainty in the achieved V_f as the fabric may not fully compress to the desired thickness. Other thickness effects arise from differences in effective permeabilities of the fabric plies inside the stack and the plies adjacent to the mold upper and lower surface, which become more apparent with reduced fabric stack thickness. Nevertheless, the variability due to thickness was found to be comparable with the conventional order of variability for linear flow experiments [23] and therefore not considered of major influence.

The overall accuracy of the CVFE method for unsaturated permeability characterization was evaluated based on several factors. Special attention had to be paid to the accuracy of measurement in the preceding random mat section since its permeability values are used to approximate the pressure distribution over the fabric length. Hence, an offset in the permeability of the random mat section alters the effective ΔP used to derive the unsaturated permeability of the fabric of interest, thereby introducing an error in the derived unsaturated permeability of that fabric. Fig. 4a shows that permeabilities of the random mat fabric showed limited scattering despite the more irregular fabric architecture compared to that of woven fabrics. Fabrics strips were cut parallel to the roll direction to limit the irregularity, while the absence of nesting also contributed to this.

A comparison between the results derived with the CVFE and SFF methods in Fig. 4a and Table 2 shows an apparent close match between the two methods. This is confirmed in Fig. 5, where the ratio of the results derived using the CVFE method to the results of the SFF method are displayed on the horizontal axis. The mismatch between the two calculation methods was typically within 15%. Fig. 5 also shows that the

CVFE method resulted in a relative underestimation in almost every case. This is attributed to how the pressure gradient was created: opening of the valve connected to the liquid inlet results in a sudden, sharp drop of the applied liquid pressure. Recovery of the pressure then takes place rapidly, in the order of seconds, but overlaps with the impregnation of the first centimeters of fabric. An example of this is shown in Supplementary Information S2. For the SFF method, the ΔP in Eq. (2) was taken as the mean pressure difference over the fabric length. The recovering liquid pressure over the first centimeters results in an underestimation of the mean ΔP for the whole fabric, which is generally significant due to the steep gradient in the pressure recovery phase. Following Eq. (2), this underestimation of ΔP would result in an overestimation of the unsaturated permeability. The CVFE method on the other hand is insensitive to this phenomenon since it considers the pressure corresponding to the individually calculated element fill times.

The unsaturated permeability of the subsequent twill weave fabric section could only be calculated by the CVFE methods since simple linear approximations on the pressure distribution do not hold when different fabric types are placed in series. A comparison could therefore only be made between the CVFE-derived unsaturated permeability and the baseline single experiments. Fig. 4b shows that unsaturated permeability experiments with fabrics placed in series were overall close to the exponential reference fit. A quantitative view on the vertical axis of Fig. 5 and in Table 2 shows that the approximations were within the conventional variability of linear flow experiments, e.g. a coefficient of variation of 30% [23,39]. The CVFE-values were however almost always lower than the reference. This is assumed not to be a result of inaccuracies in the methodology but was mainly attributed to the inhomogeneous unsaturated permeability experienced by the liquid flow in series experiments.

Saturated permeability of fabric stacks placed in series was calculated following the resistors-in-series approach of Eq. (5). The permeability of the second, twill weave, fabric section can be derived from both the overall saturated permeability and that of the preceding known random mat section. Fig. 4b shows that this method closely approximated the saturated permeability values predicted by the exponential fit for single fabrics, with only few experiments deviating significantly. An error is introduced by wrongfully ignoring the variability of the preceding random mat section, assigning a saturated permeability to this section equal to that of the single fabric exponential fit as shown in Fig. 4a while the actual saturated permeability might be slightly different. This error then directly propagates into the derived

Table 2

Overview of model system results. Note: $\pm$ means standard deviation over a minimum of 3 tests.

	Random mat					Glass weave					
	Fabric layers	Volume fraction	K_{uns} ($\times 10^{-10}$ m²)	$\frac{K_{uns,CVFE}}{K_{SFF}}$	K_{sat} ($\times 10^{-10}$ m²)	Fabric layers	Volume fraction	K_{uns} ($\times 10^{-10}$ m²)	$\frac{K_{uns,CVFE}}{K_{uns,fit}}$	K_{sat} ($\times 10^{-10}$ m²)	$\frac{K_{sat}}{K_{sat,fit}}$
1 mm	2	0.293 ±0.039	6.12 ±2.41	0.984 ±0.027	6.83 ±2.98	3	0.437 ±0.003	1.23 ±0.14	0.848 ±0.119	1.58 ±0.31	0.935 ±0.215
	2	0.327 ±0.006	3.44 ±0.33	0.915 ±0.023	3.85 ±0.34	4	0.584 ±0.002	0.19 ±0.00	0.824 ±0.008	0.26 ±0.02	0.938 ±0.066
1.8 mm	3	0.248 ±0.011	6.38 ±1.46	1.000 ±0.012	6.35 ±0.80	4	0.321 ±0.000	3.22 ±0.27	0.976 ±0.084	3.71 ±0.29	1.012 ±0.079
	3	0.244 ±0.015	8.34 ±1.75	0.978 ±0.012	6.74 ±1.25	5	0.406 ±0.003	1.04 ±0.08	0.891 ±0.105	1.31 ±0.04	1.106 ±0.015
	3	0.252 ±0.013	7.16 ±1.03	0.909 ±0.032	6.05 ±0.94	6	0.490 ±0.001	0.30 ±0.00	0.708 ±0.018	0.35 ±0.03	0.909 ±0.070
3 mm	4	0.193 ±0.037	17.1 ±6.65	0.980 ±0.040	17.4 ±6.25	8	0.380 ±0.003	2.17 ±0.20	0.882 ±0.105	2.48 ±0.24	0.991 ±0.095
	4	0.255 ±0.002	6.22 ±0.40	0.947 ±0.022	6.37 ±0.22	9	0.438 ±0.002	0.88 ±0.03	0.740 ±0.020	1.14 ±0.16	0.983 ±0.156
	4	0.271 ±0.010	4.63 ±0.35	0.937 ±0.019	5.10 ±0.74	10	0.492 ±0.002	0.49 ±0.00	0.809 ±0.020	0.63 ±0.04	1.103 ±0.079
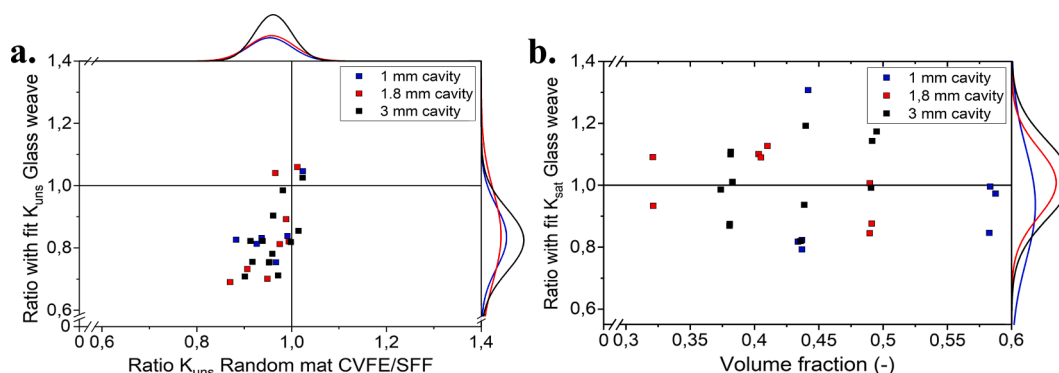
Fig. 5. Distributions and Gaussian fits of (a) Unsaturated permeability comparison CVFE method. Horizontal: the ratio between the CVFE and SFF calculated permeability of the same random mat fabric stack placed in series. Vertical: ratio of the CVFE derived permeability of the twill glass weave fabric section and the single fabric SFF reference curve. (b) Saturated permeability comparison resistors-in-series approach. Horizontal: fiber volume fraction of the twill glass weave fabric section. Vertical: ratio of series-approach derived twill glass weave fabric saturated permeability to the single reference fabric value. (For interpretation of the references to colour in this figure legend, the reader is referred to the web version of this article.)

permeability of the twill weave section, which itself is also expected to suffer from an intrinsic variability and hence a deviation from the exponential fit.

Despite this error that is intrinsic to the proposed methodology, only a limited variability of the identified permeability value was found. A quantitative view in Fig. 5b and Table 2 shows that variations were in the order of ±20% (except a single outlier with 30% deviation) with the majority of results falling within 10% of the exponential fit, while being independent of the V_f of the twill weave fabric stack. Deviations from the exponential fit were positive and negative in equal proportions. This is in contrast with the previously discussed CVFE unsaturated permeability results and due to the limited requirements on the approximation of the pressure difference (ΔP in Eq. (3)), which can be estimated from the pressure values at the extreme points of the overall fabric length. The relatively high accuracy of the resistors-in-series approach in comparison with the exponential fit can be partially attributed to the steadier character of the saturated permeability measurement. During the saturated period, the flow through the fabric can be (contrary to the unsaturated flow) averaged over a longer period of time.

After validation of the developed methodologies for unsaturated and saturated permeability determination, these were utilized to characterize the permeability of limitedly available CNT-grafted fabrics. From SEM images in Fig. 3, CNT lengths in radial- (SCNT) and 'Mohawk'-grafted (LCNT) fabrics were estimated to be 9.1 and 27 μm, respectively. The CNT length appeared to be relatively uniform within and between samples. In contrast, local uncovered spots of fiber surface were detected. For the following discussion it is therefore assumed that variations in the added weight of CNTs with similar ethylene exposure times were solely due to different degrees of fiber surface coverage by the CNTs.

Each fabric stack was built-up of three grafted fabric layers and the CNT content was aimed to be similar throughout the fabric stack. Table 3 shows that this was the case for all the used samples except for sample 'SCNT 2', which consisted of a highly grafted inner layer with

lower CNT load fabric layers on either side. The CNT load of a fabric stack was taken as the mean of that of its constituting fabrics.

Unsaturated permeability characterization of CNT-grafted fabrics is complicated by the need to estimate an effective overall fiber volume fraction during flow. This V_f accounts for the effective volume taken up by the fabric at the instantaneous moment of arrival of the infiltrating liquid. At this moment however, a number of complex phenomena are acting simultaneously. These include strong capillary action [9,40,41] that suck liquid into the available tight space between CNTs and complex CNT forest morphologies that may change in the presence of a liquid [42–44]. The timescale of these phenomena is known to be small, e.g. nanoseconds for the capillary action [40], but these may have to be taken into account at the very first arrival of the flow front as they will enhance the pressure drop, driving the flow.

Based on physical data, the analysis was carried out based on two theoretical V_f-approaches. A first approach, schematically illustrated in Fig. 6a, assumes CNTs to be fully invisible to liquid flow and the effective V_f thus equals that of the alumina fibers alone. In V_f-approach 2 (Fig. 6b) the CNTs are assumed to be solid strands that are impermeable for the liquid flow, inhibiting the liquid to pass through its center. Hence, this V_f-approach considers the volumes of the alumina fibers and that of CNTs. CNT volumes were calculated assuming perfect solid cylinders (i. e. no liquid infiltration into the inner cavity of the nanotubes) with an outer diameter of 14 nm [8], an average of eight walls and a wall spacing of 0.34 nm [18]. The resulting V_f-s are listed in Table 4.

The unsaturated and saturated permeability values of CNT-grafted fabrics are shown in Fig. 7, while a quantitative overview can be found in Table 4. Permeability values were within the typical range of 10^{-8}–10^{-12} m² for long fibrous structures [23,39,45]. CNT-grafting was found to significantly lower both permeabilities, compared to the

Table 3
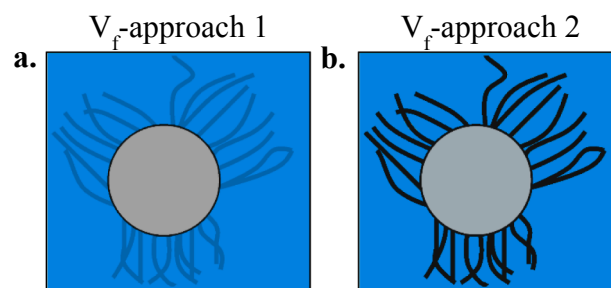Sample overview CNT-grafted samples. Note: the CNT load is defined in relation to the weight of the alumina fibers.

Sample	CNT load (wt%)		CNT load of individual layers (wt%)		
	Mean	Std. dev	Top layer	Middle layer	Bottom layer
SCNT 1	0.637	0.085	0.528	0.734	0.649
SCNT 2	0.849	0.822	0.268	2.012	0.267
SCNT 3	0.877	0.125	0.785	1.054	0.791
SCNT 4	1.301	0.068	1.281	1.393	1.229
LCNT 1	1.914	0.421	2.495	1.509	1.737
LCNT 2	4.801	0.330	4.759	4.419	5.224

Fig. 6. Theoretical volume fraction approaches: (a) $V_{f,1}$: CNTs that are invisible to flow, (b) $V_{f,1}$: Inhibited flow through CNTs. (For interpretation of the references to colour in this figure legend, the reader is referred to the web version of this article.)

Table 4

Overview of permeability results CNT-grafted fabrics. Subscript alu denotes the non-grafted alumina fabric.

Sample type and number	Unsaturated permeability					Saturated permeability		R_s
	$V_{f,1}$ (-)	K_{uns} ($V_{f,1}$) ($\times 10^{-10}$ m^2)	$V_{f,2}$ (-)	K_{uns} ($V_{f,2}$) ($\times 10^{-10}$ m^2)	$\dfrac{K_{uns}(V_{f,2}) - K_{uns,alu}}{K_{uns,alu}}$	K_{sat} ($\times 10^{-10}$ m^2)	$\dfrac{K_{sat} - K_{sat,alu}}{K_{sat,alu}}$	$\dfrac{K_{uns}(V_{f,2})}{K_{sat}}$
SCNT 1	0.206	12.3	0.208	12.0	−59.6%	4.14	−88.0%	2.89
SCNT 2	0.205	7.68	0.209	7.52	−74.5%	3.08	−90.9%	2.44
SCNT 3	0.208	5.05	0.212	4.98	−82.4%	4.38	−86.5%	1.14
SCNT 4	0.204	2.92	0.210	2.88	−90.9%	2.10	−93.7%	1.37
LCNT 1	0.125	9.81	0.130	9.63	−89.5%	7.73	−92.9%	1.25
LCNT 2	0.125	12.4	0.138	11.6	−85.8%	5.81	−94.0%	2.13
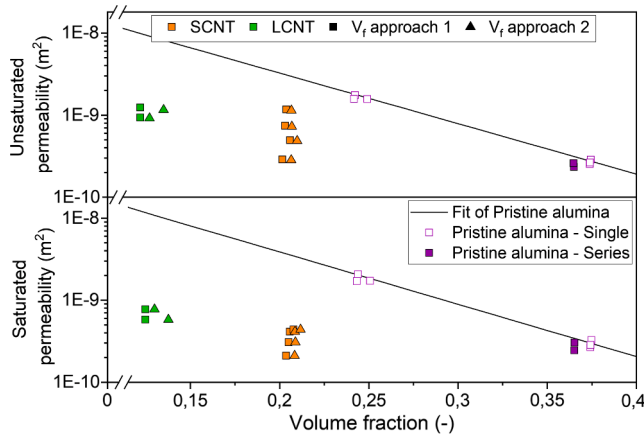
Fig. 7. Unsaturated (top) and saturated (bottom) permeability results of CNT-grafted fabrics in comparison with pristine alumina fabrics. Orange and green datapoints refer to SCNT and LCNT fabrics, respectively. Calculations based on $V_{f,1}$ are denoted by squares while triangles represent values calculated based on $V_{f,2}$. (For interpretation of the references to colour in this figure legend, the reader is referred to the web version of this article.)

pristine alumina fabric. Under the considered V_f-approaches and taking into account the respective compressibility limits [31], the radial- and 'Mohawk'-grafted fabrics were distributed as separate clusters. For that reason, the vertical shift compared to the reference curve was used as the main source of comparison between the CNT-grafted fabric types. This change in unsaturated permeability equaled −76.7 ± 11% for the radial- and −87.7 ± 1.8% for the 'Mohawk'-grafted fabric stacks. For the saturated permeability analysis, the permeability drop was even higher. Radial aligned CNT-grafting resulted in a decrease of 89.8 ± 2.8% while the presence of 'Mohawk' CNTs reduced the permeability by on average 93.4 ± 0.6%.

The observed permeability drops were in line with the observations of Refs. [28–30], who reported a strong reduction in unsaturated permeability after CNT-grafting. Moreover, they reported a stronger decrease for samples increasingly exposed to ethylene, hence with increased CNT length, which relates to the lower unsaturated permeabilities observed for 'Mohawk' CNT-grafted fabrics compared to radial aligned grafting, in agreement with our findings.

A physical explanation for the trends observed in Fig. 7 and Table 4 can be partially found in the work of Aravand et al. [19], who in their study on the microstructure of woven CNT-grafted textiles showed that grafting causes the woven tows to expand. This effect in turn causes a shrinkage of the main flow channels in-between tows, i.e. the mesochannels, and thereby a reduced fabric permeability. This was shown to increase with CNT length, hence mesochannels between the tows of 'Mohawk'-grafted fabrics are expected to be smaller than those grafted with radial aligned CNTs. A similar trend of decreasing permeability with increasing CNT load, i.e. grafting density, would also be expected between samples with the same type of grafting. Table 4 shows however

that these did not stand out, which is likely due to the limited size of the dataset combined with the high intrinsic variability of flow experiments. Nevertheless, it appeared that an inhomogeneous distribution of CNT load within a fabric stack, i.e. sample SCNT 2, does not result in permeability differences compared to homogeneously grafted fabric stacks.

The narrowing of mesochannels is thus one component of the large permeability decrease. The R_s ratios, defined as the ratio between unsaturated and saturated permeability and listed in Table 4, are always above 1 and reach up to 2.89 for sample 'SCNT 1'. These values are exceptionally high since conventional fabrics typically show values below or around 1 [34]. The R_s ratios are also significantly higher than those of the model system, which are included in Supplementary Information S4. This indicates that the systems are strongly wetting, which could be related to the capillary effects induced by the closely spaced CNT forests. R_s is however, via the unsaturated permeability, directly related to the V_f and its magnitude might result from an underestimation of the effective V_f. Nonetheless, this result is important to highlight the potential enhancement of wetting, hence of impregnation kinetics created by the presence of the CNT forests.

If the potential alteration of channel sizes due to tow expansion is ignored, the saturated permeability values, which do not involve the precise knowledge of the volume fraction in their evaluation, would be expected to match that of the pristine alumina fabric reference fit at an accurate effective V_f. It should be noted however that the presence of grafted CNTs can strongly increase the flow resistance [46], which is known to occur in highly compressed CNT-grafted fabric stacks where the CNTs bridge the major flow channels. In the current situation, however, the compressibility and the V_f are relatively low and the main inter-yarn flow channels are expected to be only partially disturbed. The extent of this was estimated by the derivation of an effective "apparent" V_f from the intersection between the measured saturated permeability of a CNT-grafted fabric and the reference fit in Fig. 7, e.g. around 0.35 for sample SCNT 1. The increase in effective fiber radius of the grafted fibers can easily be estimated from:

$$\frac{r}{r_0} = \sqrt{\frac{V_f}{V_{f,0}}} \tag{6}$$

where r is the effective fiber radius and subscript 0 indicates the non-grafted fabric. For sample SCNT 1 this would give an effective radius increase of about 29%. In the saturated flow regime, it is expected that CNT forests have already been impregnated due to the strong capillary actions induced by the closely spaced CNTs. The increased effective radius is therefore thought to represent the increased resistance experienced by the liquid flowing though CNT forests [46] in the unfavorable direction parallel to the alumina fiber surface, and thus creating additional pressure drop in the overall direction of flow [9]. A similar estimation of this for the unsaturated permeability is complicated by the time scale of events, e.g. capillary infiltration and densification of CNT forests, being unknown.

Finally, the global change in permeability of CNT-grafted fabrics compared to pristine alumina fabrics can be attributed to three main

factors: the shrinkage of mesochannels due to the expansion of grafted tows, induced capillary effects by the closely spaced CNT forests and an altered effective fiber radius. Further microscale investigations have the potential to elucidate the role of each of these factors and thereby allow for quantitative confirmation of the unsaturated and saturated permeabilities.

4. Conclusion

The present work concerned the permeability characterization of CNT-grafted fabrics. The limited sample dimensions and aspect ratios of these fabrics made characterization with use of conventional flow experiments unreliable. Instead, a series approach was employed where the fabric of interest is preceded by an isotropic random mat fabric to allow stabilization of the flow. The unsaturated permeability characterization was based on a Control Volume Finite Elements (CVFE) approach while saturated permeability was determined via a resistors-in-series approach.

Validation of the strategies was performed on a well-characterized twill weave glass fabric through comparison with the permeabilities obtained using the conventional methodologies. Accuracy of the CVFE method was found satisfactory considering the intrinsic variability of the unsaturated flow regime. The approximation for the isotropic random mat was typically within 10% of the value obtained by the conventional Squared Flow Front approach, while its underestimating character was attributed to pressure recovery during the initial impregnation stage. The unsaturated permeability of the twill weave section approached the values of single fabric experiments within 30%. The resistors-in-series approach allowed for accurate saturated permeability approximations, despite its intrinsic sensitivity for propagating errors. Saturated permeabilities of the twill weave fabric were generally within $\pm$ 10% of the values obtained in single fabric experiments, which was partially attributed to the more steady-state character of saturated permeability measurements.

The validated methodologies were applied to characterize CNT grafted woven alumina fabrics. Considered fabrics were grafted with either 9.1 μm long radial aligned CNT forests or 27 μm long 'Mohawk' CNT forests. The complex liquid flow behavior in the presence of CNT forests required the analysis to be based on theoretical fiber volume fraction (V_f) approaches. Both the unsaturated and saturated permeability were found to decrease strongly compared to the pristine alumina fabric. Decreases of 89.8 $\pm$ 2.8% for radial aligned grafting and 93.4 $\pm$ 0.6% for 'Mohawk' grafting were measured for the saturated permeability. Assuming impermeable CNTs but permeable CNT forests, the unsaturated permeability was found to decrease 76.7 $\pm$ 11% and 87.7 $\pm$ 1.8% compared to the pristine fabric after radial aligned and 'Mohawk' grafting, respectively. The quantitative unsaturated permeability results were subject to the uncertainty of the unknown V_f. From the saturated permeability data, it was reasoned that the effective fiber radius is larger than that used in the theoretical V_f-approaches, most likely due to the high flow resistance in CNT forests perpendicular to the fiber surface. Future investigation on the CNT morphology can contribute to elucidating the role of this in the liquid impregnation of CNT-grafted fabrics in combination with the shrinkage of mesochannel sizes and capillary action due to the presence of CNTs.

CRediT authorship contribution statement

Jeroen Staal: Investigation, Methodology, Validation, Writing – original draft. **Baris Caglar:** Methodology, Software, Supervision, Formal analysis, Writing – review & editing. **Travis Hank:** Investigation, Validation. **Brian L. Wardle:** Supervision, Formal analysis, Writing – review & editing. **Larissa Gorbatikh:** Conceptualization, Supervision, Writing – review & editing. **Stepan V. Lomov:** Conceptualization, Methodology, Supervision, Writing – review & editing. **Véronique Michaud:** Conceptualization, Supervision, Writing – review & editing.

Declaration of Competing Interest

The authors declare that they have no known competing financial interests or personal relationships that could have appeared to influence the work reported in this paper.

Appendix A. Supplementary material

Supplementary data to this article can be found online at https://doi.org/10.1016/j.compositesa.2021.106631.

References

[1] Zakaria MR, Md Akil H, Abdul Kudus MH, Ullah F, Javed F, Nosbi N. Hybrid carbon fiber-carbon nanotubes reinforced polymer composites: a review. Compos Part B Eng 2019;176:107313. https://doi.org/10.1016/j.compositesb:2019.107313.

[2] Keyte J, Pancholi K, Njuguna J. Recent developments in graphene oxide/epoxy carbon fiber-reinforced composites. Front Mater 2019;6:1–30. https://doi.org/10.3389/fmats.2019.00224.

[3] Yamamoto N, Wicks SS, Guzman R, Ishiguro K, Steiner SA. Mechanical, thermal, and electrical properties of woven laminated advanced composites containing aligned carbon nanotubes. In: ICCM 17th Conf. Compos. Mater.; 2009.

[4] Spitalsky Z, Tasis D, Papagelis K, Galiotis C. Carbon nanotube-polymer composites: Chemistry, processing, mechanical and electrical properties. Prog Polym Sci 2010; 35(3):357–401. https://doi.org/10.1016/j.progpolymsci.2009.09.003.

[5] Chou T-W, Gao L, Thostenson ET, Zhang Z, Byun J-H. An assessment of the science and technology of carbon nanotube-based fibers and composites. Compos Sci Technol 2010;70(1):1–19. https://doi.org/10.1016/j.compscitech.2009.10.004.

[6] Thostenson ET, Li WZ, Wang DZ, Ren ZF, Chou TW. Carbon nanotube/carbon fiber hybrid multiscale composites. J Appl Phys 2002;91(9):6034–7. https://doi.org/10.1063/1.1466880.

[7] Qian H, Greenhalgh ES, Shaffer MSP, Bismarck A. Carbon nanotube-based hierarchical composites: a review. J Mater Chem 2010;20:4751–62. https://doi.org/10.1039/c000041h.

[8] Yamamoto N, John Hart A, Garcia EJ, Wicks SS, Duong HM, Slocum AH, et al. High-yield growth and morphology control of aligned carbon nanotubes on ceramic fibers for multifunctional enhancement of structural composites. Carbon N Y 2009;47(3):551–60. https://doi.org/10.1016/j.carbon.2008.10.030.

[9] Garcia E, Wardle B, Hart A, Yamamoto N. Fabrication and multifunctional properties of a hybrid laminate with aligned carbon nanotubes grown In Situ. Compos Sci Technol 2008;68(9):2034–41. https://doi.org/10.1016/j.compscitech.2008.02.028.

[10] Qian H, Bismarck A, Greenhalgh ES, Kalinka G, Shaffer MSP. Hierarchical composites reinforced with carbon nanotube grafted fibers: the potential assessed at the single fiber level. Chem Mater 2008;20:1862–9.

[11] Veedu VP, Cao A, Li X, Ma K, Soldano C, Kar S, et al. Multifunctional composites using reinforced laminae with carbon-nanotube forests. Nat Mater 2006;5(6):457–62. https://doi.org/10.1038/nmat1650.

[12] Fidelus JD, Wiesel E, Gojny FH, Schulte K, Wagner HD. Thermo-mechanical properties of randomly oriented carbon/epoxy nanocomposites. Compos Part A 2005;36(11):1555–61. https://doi.org/10.1016/j.compositesa.2005.02.006.

[13] Fan Z, Hsiao K-T, Advani SG. Experimental investigation of dispersion during flow of multi-walled carbon nanotube/polymer suspension in fibrous porous media. Carbon N Y 2004;42(4):871–6. https://doi.org/10.1016/j.carbon.2004.01.067.

[14] Winey KI, Kashiwagi T, Mu M. Improving electrical conductivity and thermal properties of polymers by the addition of carbon nanotubes as fillers. MRS Bull 2007;32(4):348–53. https://doi.org/10.1557/mrs2007.234.

[15] Sadeghian R, Gangireddy S, Minaie B, Hsiao K-T. Manufacturing carbon nanofibers toughened polyester/glass fiber composites using vacuum assisted resin transfer molding for enhancing the mode-I delamination resistance. Compos Part A 2006;37 (10):1787–95. https://doi.org/10.1016/j.compositesa:2005.09.010.

[16] Gao S, Mader E, Plonka R. Nanocomposite coatings for healing surface defects of glass fibers and improving interfacial adhesion. Compos Sci Technol 2008;68(14):2892–901. https://doi.org/10.1016/j.compscitech.2007.10.009.

[17] Godara A, Gorbatikh L, Kalinka G, Warrier A, Rochez O, Mezzo L, et al. Interfacial shear strength of a glass fiber/epoxy bonding in composites modified with carbon nanotubes. Compos Sci Technol 2010;70(9):1346–52. https://doi.org/10.1016/j.compscitech.2010.04.010.

[18] Wicks SS, de Villoria RG, Wardle BL. Interlaminar and intralaminar reinforcement of composite laminates with aligned carbon nanotubes. Compos Sci Technol 2010; 70(1):20–8. https://doi.org/10.1016/j.compscitech.2009.09.001.

[19] Aravand MA, Shishkina O, Straumit I, Liotta AH, Wicks SS, Wardle BL, et al. Internal geometry of woven composite laminates with "fuzzy" carbon nanotube grafted fibers. Compos Part A Appl Sci Manuf 2016;88:295–304. https://doi.org/10.1016/j.compositesa:2016.06.010.

[20] Wicks SS, Wang W, Williams MR, Wardle BL. Multi-scale interlaminar fracture mechanisms in woven composite laminates reinforced with aligned carbon nanotubes. Compos Sci Technol 2014;100:128–35. https://doi.org/10.1016/j.compscitech.2014.06.003.

[21] Mehdikhani M, Gorbatikh L, Verpoest I, Lomov SV. Voids in fiber-reinforced polymer composites: a review on their formation, characteristics, and effects on mechanical performance. J Compos Mater 2019;53(12):1579–669. https://doi.org/10.1177/0021998318772152.

[22] Caglar B, Salvatori D, Sozer EM, Michaud V. In-plane permeability distribution mapping of isotropic mats using flow front detection. Compos Part A Appl Sci Manuf 2018;113:275–86. https://doi.org/10.1016/j.compositesa.2018.07.036.

[23] Vernet N, Ruiz E, Advani S, Alms JB, Aubert M, Barburski M, et al. Experimental determination of the permeability of engineering textiles: Benchmark II. Compos Part A 2014;61:172–84. https://doi.org/10.1016/j.compositesa:2014.02.010.

[24] Languri EM, Vechart A, Tan H, Pillai KM. Effect of preform aspect ratio on permeability measured through 1D flow experiments. In: 9th Int. Conf. Flow Process. Compos. Mater.; 2008.

[25] Di Fratta C, Klunker F, Trochu F, Ermanni P. Characterization of textile permeability as a function of fiber volume content with a single unidirectional injection experiment. Compos Part A 2015;77:238–47. https://doi.org/10.1016/j.compositesa.2015.05.021.

[26] Dong C. A fast permeability measurement method based on hybrid fiber preforms. Trans ASME 2005;127:670–6. https://doi.org/10.1115/1.1954794.

[27] Lomov S V, Beyers L, Gorbatikh L, Verpoest I, Koissin V, Kotanjac Z, et al. Permeability and compressibility of CNT/CNF-grafted reinforcements. In: 10th Int. Conf. Flow Process. Compos. Mater.; 2010.

[28] Lidston DL, Wicks SS, Wardle BL. Factors controlling infusion processing of laminated composites containing aligned carbon nanotubes. In: 52nd AIAA/ASME/ASCE/AHS/ASC Struct. Struct. Dyn. Mater. Conf.; 2011. p. 1–7.

[29] Wicks SS, Wang W, Wardle BL. Influence of Aligned Carbon Nanotube (CNT) Loading on Manufacturability of Hybrid Aligned CNT-Fiber Composites Through Vacuum Assisted Resin Infusion. SAMPE 2013; 2013.

[30] Wicks SS, Lidston D, Kalamoun S, Guzmán R, Wardle BL. Vacuum assisted infusion of hybrid aligned carbon nanotube-fiber composites for mechanical reinforcement. In: 18th Int. Conf. Compos. Mater.; 2011. p. 1–5.

[31] Lomov SV, Wicks S, Gorbatikh L, Verpoest I, Wardle B. Compressibility of nanofibre-grafted alumina fabric and yarns: aligned carbon nanotube forests. Compos Sci Technol 2014;90:57–66.

[32] Salvatori D, Caglar B, Teixidó H, Michaud V. Permeability and capillary effects in a channel-wise non-crimp fabric. Compos Part A 2018;108:41–52. https://doi.org/10.1016/j.compositesa.2018.02.015.

[33] Verrey J, Michaud V, Månson J-A-E. Dynamic capillary effects in liquid composite moulding with non-crimp fabrics. Compos Part A Appl Sci Manuf 2006;37(1):92–102. https://doi.org/10.1016/j.compositesa:2005.04.011.

[34] Michaud V. A review of non-saturated resin flow in liquid composite moulding processes. Transp Porous Media 2016;115(3):581–601. https://doi.org/10.1007/s11242-016-0629-7.

[35] Caglar B, Tekin C, Karasu F, Michaud V. Assessment of capillary phenomena in liquid composite molding. Compos Part A Appl Sci Manuf 2019;120:73–83. https://doi.org/10.1016/j.compositesa.2019.02.018.

[36] Pucci MF, Liotier P, Drapier S. Capillary wicking in a fibrous reinforcement – Orthotropic issues to determine the capillary pressure components. Compos Part A 2015;77:133–41. https://doi.org/10.1016/j.compositesa.2015.05.031.

[37] Levenberg K. A method for the solution of certain non-linear problems in least squares. Q Appl Math 1944;2(2):164–8.

[38] Ranganathan A. The levenberg-marquardt algorithm. Tutorial LM Algorithm; 2004.

[39] Arbter R, Beraud JM, Binetruy C, Bizet L, Bréard J, Comas-Cardona S, et al. Experimental determination of the permeability of textiles: a benchmark exercise. Compos Part A Appl Sci Manuf 2011;42(9):1157–68. https://doi.org/10.1016/j.compositesa:2011.04.021.

[40] García EJ, Hart AJ, Wardle BL, Slocum AH. Fabrication of composite microstructures by capillarity-driven wetting of aligned carbon nanotubes with polymers. Nanotechnology 2007;18(16):165602. https://doi.org/10.1088/0957-4484/18/16/165602.

[41] Lee J, Kessler SS, Wardle BL. Void-free layered polymeric architectures via capillary-action of nanoporous films. Adv Mater Interfaces 2020;7(4):1901427. https://doi.org/10.1002/admi.v7.410.1002/admi.201901427.

[42] Liu H, Li S, Zhai J, Li H, Zheng Q, Jiang L, et al. Self-assembly of large-scale micropatterns on aligned carbon nanotube films. Angew Chemie - Int Ed 2004;43 (9):1146–9.

[43] Zhang R, Zhang Y, Wei F. Horizontally aligned carbon nanotube arrays: Growth mechanism, controlled synthesis, characterization, properties and applications. Chem Soc Rev 2017;46(12):3661–715. https://doi.org/10.1039/C7CS00104E.

[44] Kaiser AL, Stein IY, Cui K, Wardle BL. Process-morphology scaling relations quantify self-organization in capillary densified nanofiber arrays. Phys Chem Chem Phys 2018;20(6):3876–81. https://doi.org/10.1039/C7CP06869G.

[45] Michaud V. Permeability properties of composite reinforcements. Compos. Reinf. Optim. Perform. 2021:443–72. https://doi.org/10.1016/B978-0-12-819005-0.00014-9.

[46] Shahsavari S, Wardle BL, McKinley GH. Interception efficiency in two-dimensional flow past confined porous cylinders. Chem Eng Sci 2014;116:752–62. https://doi.org/10.1016/j.ces.2014.05.054.